Nucleic Acids Research Advance Access published July 12, 2010

Nucleic Acids Research, 2010, 1–11
doi:10.1093/nar/gkq598

Torsional sensing of small-molecule binding using magnetic tweezers

Jan Lipfert, Sven Klijnhout and Nynke H. Dekker*

Department of Bionanoscience, Kavli Institute of Nanoscience, Delft University of Technology, Lorentzweg 1, 2628 CJ Delft, The Netherlands

Received May 4, 2010; Revised June 5, 2010; Accepted June 17, 2010

ABSTRACT

DNA-binding small molecules are widespread in the cell and heavily used in biological applications. Here, we use magnetic tweezers, which control the force and torque applied to single DNAs, to study three small molecules: ethidium bromide (EtBr), a well-known intercalator; netropsin, a minor-groove binding anti-microbial drug; and topotecan, a clinically used anti-tumor drug. In the low-force limit in which biologically relevant torques can be accessed ($<$10 pN), we show that ethidium intercalation lengthens DNA $\sim$1.5-fold and decreases the persistence length, from which we extract binding constants. Using our control of supercoiling, we measure the decrease in DNA twist per intercalation to be 27.3 ± 1° and demonstrate that ethidium binding delays the accumulation of torsional stress in DNA, likely via direct reduction of the torsional modulus and torque-dependent binding. Furthermore, we observe that EtBr stabilizes the DNA duplex in regimes where bare DNA undergoes structural transitions. In contrast, minor groove binding by netropsin affects neither the contour nor persistence length significantly, yet increases the twist per base of DNA. Finally, we show that topotecan binding has consequences similar to those of EtBr, providing evidence for an intercalative binding mode. These insights into the torsional consequences of ligand binding can help elucidate the effects of small-molecule drugs in the cellular environment.

INTRODUCTION

The interaction of DNA with ligands is fundamental for many cellular processes, including transcription and replication. When these ligands constitute low-molecular weight organic compounds, they are generally referred to as 'small molecules'. Such small molecules, which are either naturally occurring or chemically synthesized, can partake in cellular processes such as signaling, but they are also employed in a range of biotechnological applications, e.g. DNA staining, as well as in a range of therapeutic applications, e.g. in cancer therapy and as antimicrobial drugs. Small molecules employ a variety of different DNA binding modes such as intercalation (1), minor groove binding and major groove binding (2–5). Recently, advances in single-molecule manipulation techniques have made possible the study of DNA–ligand interactions at the single molecule level. For instance, force spectroscopy experiments which can modulate the stretching force on nucleic acids have investigated small molecule binding both using optical tweezers (OT) (4,6–16) and atomic force microscopy (AFM) (3,5,17). Similarly, the passage of individual DNA molecules through small apertures known as solid-state nanopores, allowing one to probe its conformation, can likewise detect the presence of small molecules (18). These techniques offer the possibility of very precise, real-time detection on minute sample quantities.

The primary mode in which single-molecule experiments have been used to probe the mechanical properties of single DNA molecules in the presence of DNA-binding ligands is through the modulation of the stretching force and simultaneous measurement of the DNA extension. Single-molecule stretching experiments have provided unique insights into how various ligands change the force–extension properties of DNA (10,11,19). In turn, such measurements can inform us about properties of the ligands, for example they can be used to discern different binding modes (4,5). In the cellular environment, however, not only DNA stretching in response to force, but in particular also twisting and supercoiling of DNA in response to torque are important parameters that control the properties of cellular DNA. Supercoiling of DNA in the cell is tightly regulated by topoisomerases (20,21) and is suggested to play a role in gene regulation (22,23). The twist and writhe of the DNA double helix that accompany supercoiling can occasion structural changes in the DNA

*To whom correspondence should be addressed. Tel: +31 152 783 219; Fax: +31 152 781 202; Email: n.h.dekker@tudelft.nl

(24–29). Using single-molecule techniques to precisely probe the effect of supercoiling on the binding of small molecules, which are known to be sensitive to the shape of the double-helix, could prove to be a particularly sensitive tool to detect small molecule binding and have the potential to provide unique insights in the interplay of torque and DNA–ligand interactions.

In this work, we present results using single molecule magnetic tweezers (MT; Figure 1A) measurements to probe the mechanical properties of DNA-binding ligands under force and torque. In particular, we study three different molecules: ethidium bromide (EtBr), which is a known DNA intercalator (Figure 1B) (30) employed in the staining of DNA molecules during gel electrophoresis; netropsin (31–33), an oligopeptide with anti-microbial activity that binds in DNA's minor groove (Figure 1C) (34–36); and topotecan (TPT; Figure 1D), a camptothecin-analogue and topoisomerase IB inhibitor that is in clinical use as a chemotherapeutic (37–39). For topotecan, both minor groove binding (40,41) and intercalation (42) have been suggested as interaction modes with bare DNA. Our approach is to study in depth the parameters that can be extracted from our single-molecule approach using EtBr as a model system, and then, to demonstrate the versatility of the approach, extend it to the cases of netropsin and TPT. In the case of TPT, where the mode of binding has been controversial, our results indicate an intercalative binding mode.

MATERIALS AND METHODS

We use a MT setup similar to that previously described (Figure 1A) (43,44). Briefly, a CCD camera with a sampling frequency of 120 Hz is used to track 1.0 μm diameter, streptavidin-coated superparamagnetic beads (Dynabeads MyOne, Invitrogen-Life Technologies) tethered to the surface by single DNA molecules. As tethers, we employ a 20.6-kb dsDNA construct with 0.6-kb handles on both ends containing multiple biotin and digoxigenin labels, respectively (43). Flow cells are made from microscope coverslips with parafilm spacers. The bottom surfaces are coated with polystyrene and functionalized with anti-digoxigenin antibodies. Prior to the measurements, surfaces are passivated with bovine serum albumin (BSA; 10 mg/ml). Reference beads are attached to the surface and imaged simultaneously with the measurement beads to correct for mechanical drift. Bead positions are tracked in x, y and z with an accuracy of ~5 nm. As magnets, we use gold-plated (Ni–Cu–Ni–Au), $5 \times 5 \times 5\,mm^3$ neodymium-iron-boron (NdFeB) permanent magnets (SuperMagnete, Germany) (45).

Measurements with EtBr and netropsin are performed in phosphate buffered saline (PBS, 137 mM NaCl, 2.7 mM KCl, 10 mM phosphate buffer, pH 7.4) supplemented with 100 μg/ml BSA, 0.1% Tween and 5 mM sodium azide. Measurements with TPT are performed in 10 mM Tris–HCl buffer, pH 7.4, similarly supplemented with

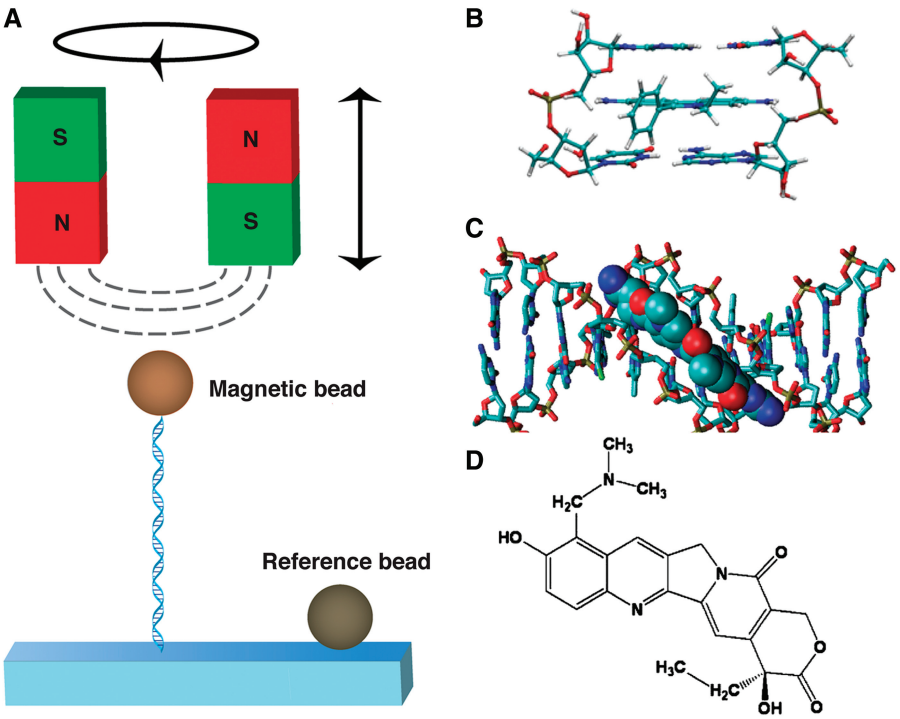

Figure 1. Experimental schematic and the structure of the small molecules under study. (**A**) Magnetic tweezers experimental configuration, in which a single DNA molecule is tethered between a superparamagnetic bead on one side, and to a glass surface on the other side. The tethering occurs via multiple attachment points, rotationally constraining the DNA. (**B**) Crystal structure of ethidium intercalated in double-stranded DNA [adopted from (30)]. (**C**) Crystal structure of netropsin bound in the minor groove of double-stranded DNA [(36); PDB accession code 101D; figure was rendered using VMD (72)] (**D**) Chemical structure of topotecan. As there is no crystallographic structure of TPT bound to bare DNA and as the binding mode of topotecan to double-stranded DNA in the absence of topoisomerase IB is under dispute (see main text), we display the chemical structure of the molecule alone.

100 µg/ml BSA, 0.1% Tween and 5 mM sodium azide. Measurements with a specific buffer and drug concentration are initiated by pumping at least 300–400 µl (= 3–4 cell volumes) of the appropriate solution through the flow cell and waiting for several minutes to allow for equilibration. We find DNA-binding to be reversible for all three drugs investigated as judged from the fact that the DNA force–extension and rotation–extension behavior (see 'Results and discussion' section) returns to that of bare DNA after extensively flushing the flow cell with buffer solution without any drug added (data not shown). However, complete removal of the drugs from the flow cell requires extensive flushing (>2 ml buffer and >30 min time), which may be due to the intrinsic dissociation times of the drugs from DNA or due to residual drug concentrations in the flow cell after initial flushing. To ensure good control over the effective drug concentration, all measurements shown are initiated with DNA molecules in the absence of drug and the drug concentration is only increased for subsequent measurement with the same flow cell.

RESULTS AND DISCUSSION

The binding of small molecule ligands was investigated by measuring their effect on the mechanical properties of DNA, which can be monitored either by varying the force on DNA and measuring the corresponding extension, or by varying the degree of supercoiling of the DNA and again measuring the corresponding extension. We performed these measurements for three types of small molecules: ethidium bromide (Figure 1B), which we employed as our model small molecule, followed by netropsin (Figure 1C) and topotecan (Figure 1D).

DNA force–extension response in the presence of varying concentrations of EtBr

We first performed DNA stretching experiments in the presence of increasing concentrations of EtBr on torsionally relaxed DNA. We ensured that the DNA was torsionally relaxed by recording rotation–extension curves for each EtBr concentration at a stretching force of $F = 0.25$ pN and adjusting the magnet rotation to center the rotation curve; this procedure is described in detail in the section 'Rotation–extension response of DNA under different stretching forces in the absence and presence of EtBr' below. The experiments for torsionally relaxed DNA are analogous to measurements by optical tweezers or AFM and allow for direct comparison of the methods. As shown in Figure 2A, we focused on the low-force limit below 10 pN for our force–extension measurements: This is the regime in which biologically relevant torques can be accessed following application of supercoiling (28) and in which the DNA extension is well described by the worm-like chain (WLC) model of entropic stretching elasticity (46). Shown in dark blue is the typical response of dsDNA to force in the absence of drug. A fit to the WLC model (47) (Figure 2A, solid dark blue line) yields values of the contour length $L_C = 7.1 \pm 0.2$ µm (mean and standard deviation from 12 independent measurements), in close agreement with the expected crystallographic length of 7.0 µm expected for a 20.6-kb dsDNA. For the bending persistence length we found $L_P = 47 \pm 3$ nm, in agreement with

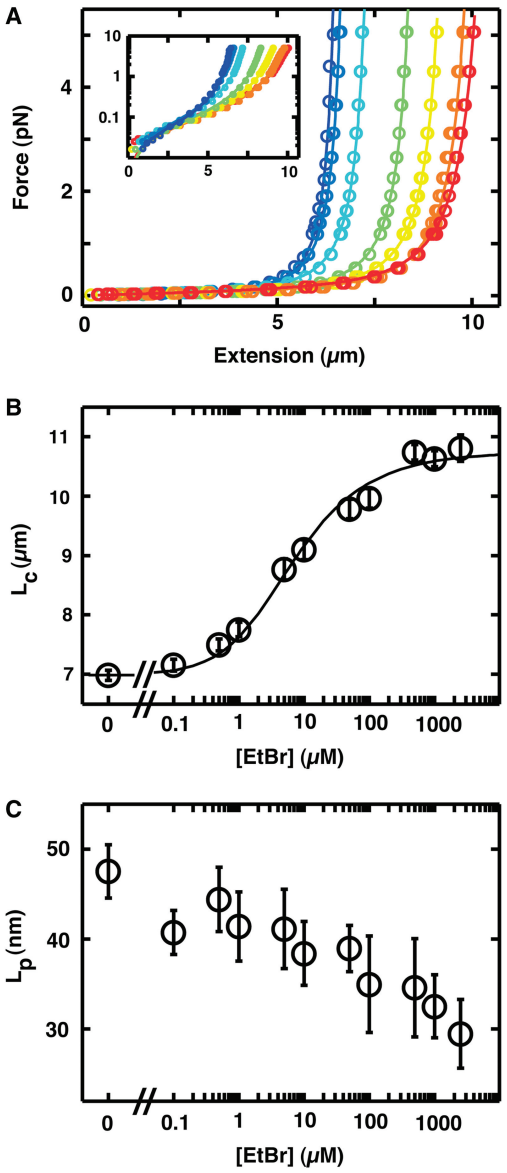

Figure 2. Effect of EtBr on DNA force–extension curves. (**A**) Force–extension curves for 20.6-kb DNA in the presence of increasing concentrations of EtBr. EtBr concentrations employed are (from blue to red) 0, 0.1, 1, 10, 100, 1000 and 2500 µM. In the absence of EtBr, we determine $L_C = 7.1 \pm 0.2$ µm and $L_P = 47 \pm 3$ nm for this 20.6-kb DNA from fits of the WLC model, in accordance with literature values (see main text). Upon addition of EtBr, it is readily observed that the DNA extension increases. (**B**) The DNA contour length L_c determined from fits of the WLC model measured as a function of EtBr concentration. The black line is a fit to the McGhee–von Hippel model (see main text for details), with a binding constant $K \approx 1.3 \times 10^5\,M^{-1}$ and binding site size $n \approx 1.9$. (**C**) The DNA bending persistence length L_P from WLC fits as a function of EtBr concentration, indicating that the bending persistence length decreases with increasing [EtBr]. Data in panels B and C are the mean and standard deviation from at least three independent measurements. In panel A one typical experiment is shown for clarity.

previous measurements under similar buffer conditions (45,48). We then added increasing concentrations of EtBr (Figure 2A, curves from lightblue to red). At any given concentration, force–extension curves could be repeated over the given force range without a change in the response of the molecule. The concentration of EtBr was then increased prior to a subsequent measurement. One can readily observe that the contour length of the molecule increases as the EtBr concentration is increased: compared to the contour length of bare DNA, the contour length of DNA in the presence of 2500 μM EtBr increases ~50%. This observation is in agreement with previous work using AFM and optical tweezers (5,9,49–51). At this latter concentration, the increase in the contour length is nearly maximal, as can also be seen from the plot of contour length versus EtBr concentration shown in Figure 2B. In addition to undergoing an increase in its contour length following ethidium binding, the DNA molecule also adapts its bending rigidity, as is shown in Figure 2C where we plot the bending persistence length versus the EtBr concentration. We observe a steady decrease in the bending persistence length of DNA as the EtBr concentration is increased to 2500 μM.

From the mechanical response of ethidium-bound DNA to force, we can extract precise biochemical parameters such as the binding constant and binding site size. For this we employ the McGhee–von Hippel model of ligand-substrate binding (52), which provides the following equation for the fractional number of molecules bound per base pair, γ:

$$\gamma = CK\frac{(1-n\gamma)^n}{(1-n\gamma+\gamma)^{n-1}}$$

where C is the ligand concentration, K is the binding constant (in M^{-1}) and n is the binding site size (in base pairs). If we assume that the binding of an ethidium molecule increases the dsDNA contour length by Δz_{EtBr}[which has been measured to equal 0.34 nm (53)], the number of bound ethidium molecules given an observed contour length L_C is equal to $(L_C([EtBr]) - L_C([0]))/\Delta z_{EtBr}$, and hence γ equals $(L_C([EtBr]) - L_C([0]))/\Delta z_{EtBr} N_{bp}$. The data of L_C versus [EtBr] is well described by the resulting McGhee–von Hippel relation (Figure 2B; reduced χ^2 of the fit = 1.09) and we extract a binding constant (association constant) $K = (1.3 \pm 0.4) \times 10^5\,M^{-1}$ and a binding site size $n = 1.9 \pm 0.1$. The value of the binding constant compares favorably to results from optical tweezers experiments in a high-force regime (10), which yielded $K = 4.6 \times 10^5\,M^{-1}$ and $n = 2.4$ and to results from a rotary bead assay in the absence of stretching force (54) that resulted in fitted values of $K = 1.2 \times 10^5\,M^{-1}$ and $n = 1.8$. Similarly, an experiment monitoring EtBr-binding to DNA in solid-state nanopores yielded a value of the dissociation constant K_d of ~15 μM, corresponding to a binding constant of $\sim 7 \times 10^5\,M^{-1}$ (18). The value of the binding site size n can be interpreted as ethidium intercalation maximally occurring approximately every other basepair (55).

Considering the dependence of the bending persistence length on the EtBr concentration, we can estimate a binding constant $K \sim 10^5\,M^{-1}$ by determining the EtBr concentration at which the change in the persistence length is at the midpoint of its range. However, the quantitative conversion from a change in bending persistence length to a number of DNA bases bound with ethidium is not straightforward, preventing us from independent fitting to the McGhee–von Hippel model.

Effect of varying concentrations of EtBr on torsionally constrained DNA

We next performed experiments on rotationally constrained single molecules of DNA, as this permitted us to view the effect of ethidium binding on DNA twist. For the torsionally constrained DNA in our MT assay, we control the linking number Lk by rotation of the magnets. The linking number is equal to the sum of twist Tw and writhe Wr: $Lk = Tw + Wr$ (44,56). Tw is the number of helical turns in the double helix and Wr is the number of times the double helix crossed itself. For a torsionally relaxed bare DNA molecule $Tw = Tw_0$ and $Wr = 0$, where Tw_0 is the natural twist of DNA, equal to number of base pairs divided by the helical pitch, ~10.5 bp per turn.

Monitoring the extension as a function of magnet turns at a low fixed force of $F = 0.25$ pN, we observe the characteristic response of bare DNA (Figure 3A, dark blue symbols): Initially the change in Lk leads to elastic deformations of the DNA and a change in Tw. Subsequently, the DNA buckles to form plectonemic supercoils and the further increase of Lk is absorbed by an increase in Wr, resulting in a linear reduction of its end-to-end extension with increasing number of turns (Figure 3A, dark blue line). At this low force ($F = 0.25$ pN) the response of the DNA is symmetric about Lk_0 (or zero applied turns): applying positive or negative turns leads to formation of positive or negative supercoils, respectively.

After flushing in buffer with a fixed concentration of EtBr, we observe a very rapid decrease in the distance of the magnetic bead from the glass surface, indicating a reduction of the DNA end-to-end extension. However, rotation of the magnets towards negative turns, which reduces Lk, leads to a subsequent increase in the length of the tether, recovering qualitatively the typical symmetric response of a DNA molecule to rotation, but at a reduced linking number Lk_0([EtBr]). As the EtBr concentration is subsequently further increased, again the apparent tether length is reduced, but it can again be recovered by further reducing Lk, as is observed in Figure 3A as one follows the curves from blue to red. We observe that at the highest EtBr concentration employed, 2500 μM, the maximum of the rotation–extension curve is shifted by more ~900 rotations compared bare DNA. Closer inspection of these curves additionally reveals an increase of their maximum extension with increasing EtBr concentration, consistent with the lengthening observing during stretching experiments with

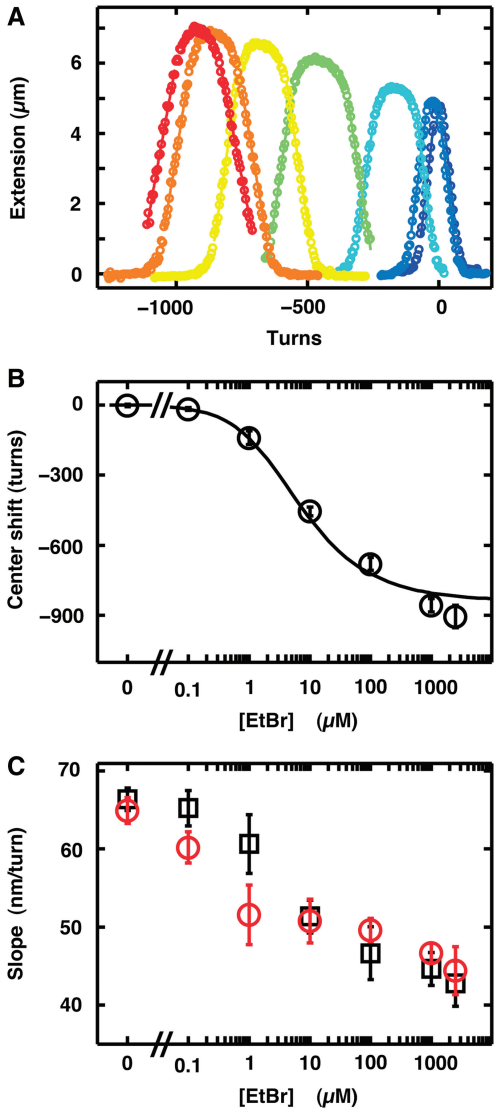

Figure 3. Effect of EtBr on DNA rotation–extension curves at low force. (**A**) Rotation–extension curves for 20.6-kb DNA in the presence of increasing concentrations of EtBr, taken at $F = 0.25$ pN. EtBr concentrations employed are (from blue to red) 0, 0.1, 1, 10, 100, 1000 and 2500 μM. Upon addition of EtBr, it is observed that rotation of the magnets to negative turns is required to recover the maximum of the rotation–extension curves, that the DNA length at this maximum increases, and that the rotation–extension curves adopt a broader shape with reduced slopes in the plectonemic regime. (**B**) Quantification of the number of negative turns required to recover the maximum of the rotation–extension curves in the presence of EtBr, as a function of the EtBr concentration. From a fit to the McGhee–von Hippel model (black line; see main text for details), we determine the unwinding angle per ethidium intercalation event to be 27.3 ± 1°. (**C**) Quantification of the slopes of the rotation–extension curves in the plectonemic regime in the presence of EtBr, as a function of the EtBr concentration. Slopes are analyzed in the plectonemic regime for positive supercoils (black) and negative supercoils (red). Data in panels B and C are the mean and standard deviation from at least five independent measurements. In panel A one typical experiment is shown for clarity.

rotationally relaxed molecules. In addition, we detect a broadening of the width of the curves and a decrease in the slope of the curves in the plectonemic regime. We now discuss these effects in more detail.

We can understand the shift in the center of the rotation–extension curves following the addition of EtBr by realizing that our DNA molecules are rotationally constrained: in that case, if the binding of a small molecule occasions a change in the DNA Tw, compensatory changes in Wr must occur (since for a fixed magnet rotation Lk is constant). Changes in Wr, which is zero for the case of relaxed DNA, result in a reduction of the DNA end-to-end extension. Ethidium intercalation is known to unwind the DNA, i.e. reduce its Tw (57). Wr must therefore increase, decreasing the DNA end-to-end extension, as observed in our experiments. Subsequent rotation of the magnets towards negative turns reduces both Lk and Wr, and leads to an increase in the DNA extension, which peaks at the value of ΔTw induced by the binding of the ethidium molecules. Plotting the shift in the rotation curve centers versus the EtBr concentration (Figure 3B; data are the mean and standard deviation from at least five independent measurements), we observe a binding curve similar to that determined from the DNA extension. Using the values for K and n determined from the stretching experiments (Figure 2), we can again fit the McGhee–von Hippel model, but now with the change in twist per intercaleted ethidium molecule $\Delta Tw_{\mathrm{EtBr}}$ as a free parameter. From the fit, we find $\Delta Tw_{\mathrm{EtBr}} = 27.3 \pm 1°$ (reduced $\chi^2 = 1.6$), in excellent agreement with the value determined from bulk studies of $26 \pm 3°$ (57). Alternatively, we can take the literature value $\Delta Tw_{\mathrm{EtBr}} = 26 \pm 3°$ as given and fit K and n to the shift in center position, yielding $K = (0.9 \pm 0.1) \times 10^5\,\mathrm{M}^{-1}$ and $n = 1.7 \pm 0.2$, in good agreement with the independently fitted values from the contour length data.

In the plectomic region, the extension in the rotation–extension curves decreases linearly with the number of turns (Figure 3A, solid lines). The fitted slopes, i.e. the reduction in length per turn Δz, decrease with increasing concentration of EtBr (Figure 3C). We can understand this behavior qualitatively by considering a simple elastic model of DNA mechanics (44,56). We note that the simple elastic model makes a number of simplifying assumptions and describes experimental data only approximately [≤25% error in the force range considered here (44,48)]. Nonetheless, this simple model is useful to explore the observed trends since it has a minimum number of parameters and does not require a numerical solution, unlike more sophisticated models of DNA supercoiling [e.g. (58–60)]. The simple model predicts that the size of a plectonemic supercoil scales as the square root of the persistence length: $\Delta z \sim \sqrt{L_{\mathrm{P}}}$ (44,56). Thus, given the persistence length of 47 nm measured in the absence of EtBr as well as the persistence length of 29 nm measured at saturating concentration of EtBr (Figure 2B), this simple model predicts a reduction of the slopes of the rotation–extension curves in the plectonemic regime of $\Delta z(0\,\mathrm{mM})/\Delta z(2.5\,\mathrm{mM}) = (47/29\,\mathrm{nm})^{1/2} \sim 1.3$, compared to the observed change in the slopes $\Delta z(0\,\mathrm{mM})/\Delta z(2.5\,\mathrm{mM}) \sim 1.5$. The simple elastic model captures the right trend, but quantitatively underestimates the change in the plectoneme slope, which may be a consequence of simplifying assumptions employed in the model. From the dependence of the slopes of the rotation–extension curves

versus increasing EtBr concentration, we can estimate a binding constant from the concentration at which the extent of the change in the slopes is at the midpoint of its range, $[EtBr]_{1/2} \sim 10\,\mu M$. This midpoint is in good agreement with the binding constants determined from the changes in L_C or the shift of the rotation curve centers. However, as in the case of the bending persistence length, the conversion from a change in slope to a number of ethidium molecules intercalated is not straightforward, and, therefore, we did not attempt to fit the slope data to the McGhee–von Hippel equation independently.

Rotation–extension response of DNA under different stretching forces in the absence and presence of EtBr

To yield further insight into the effects of ethidium binding to DNA, we carried out rotation–extension experiments at different stretching forces in the absence of EtBr (Figure 4A, shading darkens with increasing force) and at saturating concentrations of EtBr (Figure 4B, same color code as 4A). At forces below 1 pN (lowest two curves in Figure 4A), rotation–extension curves in the absence of EtBr are symmetric and exhibit a buckling transition and a linear decreases in the extension with increasing turns at both positive and negative turns. Buckling transitions at positive turns are indicated by the dashed vertical lines in Figure 4A. At forces above ~1 pN, bare DNA does not buckle when underwound but denatures locally instead (27,61), which results in the absence of a significant decrease of the tether length at negative turns (Figure 4A, five highest curves). At forces above ~6 pN, DNA ceases to buckle even when overwound due to the formation of P-DNA (27), an alternative conformation of the DNA helix, causing the rotation–extension curves to look approximately flat (Figure 4A, highest two curves).

The response of DNA in the presence of saturating concentrations of EtBr to changes in its linking number at various forces is shown in Figure 4B. For easy of comparison, the rotation–extension curves at saturating EtBr concentration have been shifted by centering the lowest force curve ($F = 0.25$ pN) to zero turns. Without this offset, the center of the curve at $F = 0.25$ pN and [EtBr] = 2.5 mM is at ~−900 turns (Figure 3), making it difficult to directly compare to the data recorded in the absence of EtBr. The turn-offset determined for the $F = 0.25$ pN curve was then applied uniformely to the data taken at higher force values.

Comparing the rotation–extension curves at different forces at saturating EtBr concentration (Figure 4B) to the bare DNA data (Figure 4A), we observe several differences, most notably: (i) a significant broadening of the curves (which was already observed at $F = 0.25$ pN in Figure 3A); (ii) a corresponding increase in the number of rotations (change in Lk) that need to be aplied to induce buckling and the formation of plectonemic supercoils (vertical lines in Figure 4 indicate buckling transitions at positive turns); (iii) the appearance of a slope in the region near the peak of the rotation–extension curve, which in the case of bare DNA is typically flat; (iv) continued buckling of the molecule at negative turns

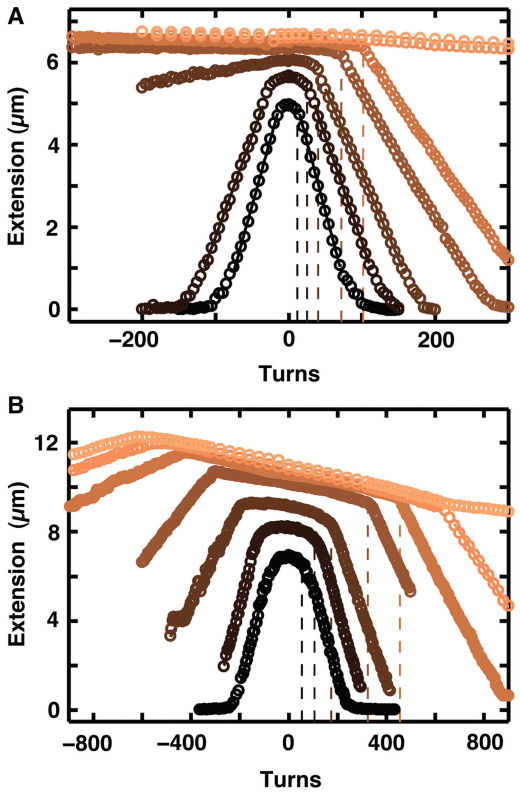

Figure 4. Effect of saturating EtBr on the response of DNA to rotation. (**A**) Rotation–extension curves for 20.6-kb DNA in PBS at different forces, in the absence of EtBr. The forces employed are (dark to light): 0.25, 0.5, 1, 3, 5, 7 and 10 pN. (**B**) Rotation–extension curves for 20.6-kb DNA in PBS at different forces, in the presence of a saturating concentration of EtBr (2500 μM, see Figures 2 and 3). Same forces and color code as in panel A. These curves are offset such that the center is at zero turns according to the procedure described in the main text, for ease of comparison. Ethidium binding causes a number of changes in the rotation–extension curves, see main text for details. For each force value one representative rotation curve is shown in panels A and B for clarity; however, at least three independent measurements for each force gave identical results, within experimental error.

(large decrease in Lk) as opposed to denaturation at all forces; and (v) buckling at positive turns (large increase in Lk) at forces at which the buckling transition for bare DNA is suppressed (cf. data at 7 pN in Figure 4). We now discuss these observations in turn.

We first discuss the broadening of the rotation–extension curves in the presence of saturating [EtBr], which, by comparing the x-axis in Figure 4A and B, occurs over the entire force range examined (0.25–10 pN). Vertical lines in Figure 4A (B) designate the number of turns n_b^{DNA} (n_b^{EtBr}) that must be applied to the relaxed DNA (relaxed DNA with EtBr) in order to induce buckling and plectonemic supercoiling at positive turns. By noting where the lines intersect the x-axis, we can readily see that buckling of the DNA in the presence of saturating EtBr occurs at $n_b^{EtBr} > n_b^{DNA}$. Numerically, we find $n_b^{DNA} = 12$, 25, 40, 72 and 102 at $F = 0.25$, 0.5, 1, 3 and 5 pN, compared to $n_b^{EtBr} =$ 55, 105, 175, 325 and 455 at the same forces, yielding a ratio of n_b^{EtBr}/n_b^{DNA} ~4.5 across all forces.

There are a number of ways of interpreting this finding. Fundamentally, a molecule will buckle if the energy required to form plectonemes becomes less than the energy stored in the elastic strain induced by additional turns. Employing again the simple elastic model for DNA introduced above (44,56), the buckling torque is approximately given by $\Gamma_b = \sqrt{kTL_PF}$. Prior to the buckling transition, the torque builds up linearly with the number of turns n according to $\Gamma = (2\pi C/L_C)n$, where C is the torsional stiffness of the molecule, until the buckling torque is reached at $n = n_b$. Thus, the increased number of turns required to observe buckling in the presence of saturating [EtBr] may be interpreted as a decrease in the torsional stiffness of DNA in the presence of saturating [EtBr], according to: $\left(C^{EtBr}/C^{DNA}\right) = \left(L_C^{EtBr}/L_C^{DNA}\right)\left(n_b^{DNA}/n_b^{EtBr}\right)\sqrt{\left(L_P^{EtBr}/L_P^{DNA}\right)}$. Plugging numerical values into this expression ($L_C^{DNA} = 7.1\,\mu m$, $L_C^{EtBr} = 10.8\,\mu m$, $n_b^{DNA}/n_b^{EtBr} \sim 0.22$, $L_P^{DNA} = 47\,nm$ and $L^{EtBr} = 29\,nm$), we obtain $C^{EtBr}/C^{DNA} \approx 0.26$, indicating that the observed shift in the buckling transition could be explained by an ~4-fold reduction in the torsional stiffness of DNA when bound by saturating concentrations of EtBr.

However, a second effect that likely contributes to the broadening of the rotation–extension curves and to the shift in the buckling points upon addition of EtBr is a torque dependence of ethidium binding. Examination of the plateau regions in the rotation–extension curves about Lk_0([EtBr]) reveals a negative slope at saturating [EtBr], an effect that is particularly pronounced at higher forces (compare Figure 4A and B, lighter traces). Here, the end-to-end extension of the DNA increases as negative turns are applied and decreases as positive turns are applied. Interestingly, the extension is maximal not at the center of the rotation–extension curve, as is the case for bare DNA, but at negative turns, i.e. at a reduced linking number. As length changes can be associated with ethidium binding to the DNA duplex, these observations suggest that the application of a negative torque stimulates ethidium binding, whereas the application of a positive torque disrupts ethidium binding, i.e. this suggests a torque-dependent binding constant (62) [$K = K_0 \exp(-\tau\theta/kT)$], similar to the observations for a force-dependent binding constant at forces exceeding 5 pN (10). Given that ethidium unwinds the DNA helix (Figure 2), it seems plausible by Le Chatelier's principle that overwinding or positive torque should hinder binding while underwinding or negative torque would promote binding. The explanation for why we observe $n_b^{EtBr} > n_b^{DNA}$ can also be re-examined in light of this observation: at positive torques, it may be possible to decrease the torsional strain due to the overwinding of the ethidium-bound DNA by unbinding of ethidium molecules, which changes the equilibrium helicity of the molecule. Conversely for negative torques it may be possible to decrease the twist by accommodating the intercalation of additional ethidium molecules, which unwind the DNA (Figure 2). Both processes would decrease the torsional energy stored in the molecule and delay the transition to either buckling or denaturation. This provides an alternative explanation to the decrease of the torsional stiffness C for the broadening of the rotation–extension curves in the presence of EtBr. We note, however, that it is likely that both a decrease in C and torque-dependent binding contribute to the observed broadening, which future experiments should be able to unravel in greater detail.

The last feature of the data in Figure 4 that we discuss are the wings of the rotation–extension curves at high forces in which Lk deviates the most from Lk_0, which inform us about structural transitions of DNA. For bare DNA (Figure 4A), we observe that at positive torques twist accumulation is followed by buckling and a decrease in tether extension up to forces of ~6 pN, but that at negative torques the same behavior is only observed at lower forces. At forces of 1 pN and higher, the molecule's extension at negative turns either decreases less rapidly or stays nearly flat, a behavior that is associated with a critical torque for denaturation that is lower than the critical torque for buckling, which results in the formation of denatured regions in the DNA duplex (27,61). At a force of 1 pN, an equilibrium between buckling and denaturation is formed, whereas at higher forces, denaturation dominates. In the presence of saturating concentrations of EtBr (Figure 4B), we observe that buckling, as evidenced by a reduction in DNA end-to-end extension, is still observed at negative supercoiling even for forces as high as 10 pN, a regime where bare DNA denatures. As above, we can argue that the critical torque for buckling should not differ greatly in the presence or absence of EtBr, due to the relatively weak (square root) dependence on changes in the bending persistence length. Thus, the continued observation of buckling in the presence of EtBr therefore argues that the critical torque for denaturation must have increased in the presence of ethidium binding. Alternatively stated, ethidium intercalation suppresses the melting transition at $F > 1$ pN and negative torque, and thus the binding of ethidium stabilizes dsDNA over ssDNA. This is in line with observation that increasing concentrations of EtBr help to suppress the DNA overstretching transition at $F > 50$ pN (6,9), which has been shown to involve DNA melting (63,64).

The presence of EtBr also appears to suppress the transition from B-form DNA to P-form DNA. In the absence of EtBr, DNA does not buckle at positive turns at forces above ~6 pN (Figure 4A, two highest curves) and instead undergoes a transition to P-DNA (27,65). In contrast, in the presence of saturating concentrations of EtBr we observe buckling at positive turns at 7 pN (Figure 4B, second curve from the top) suggesting that the presence of EtBr stabilizes the B-form of DNA relative to its P-form.

Effects of the minor groove binder netropsin on torsionally constrained DNA

The above experiments show how single-molecule manipulation including the application of torque can unravel the binding behavior of ethidium molecules to

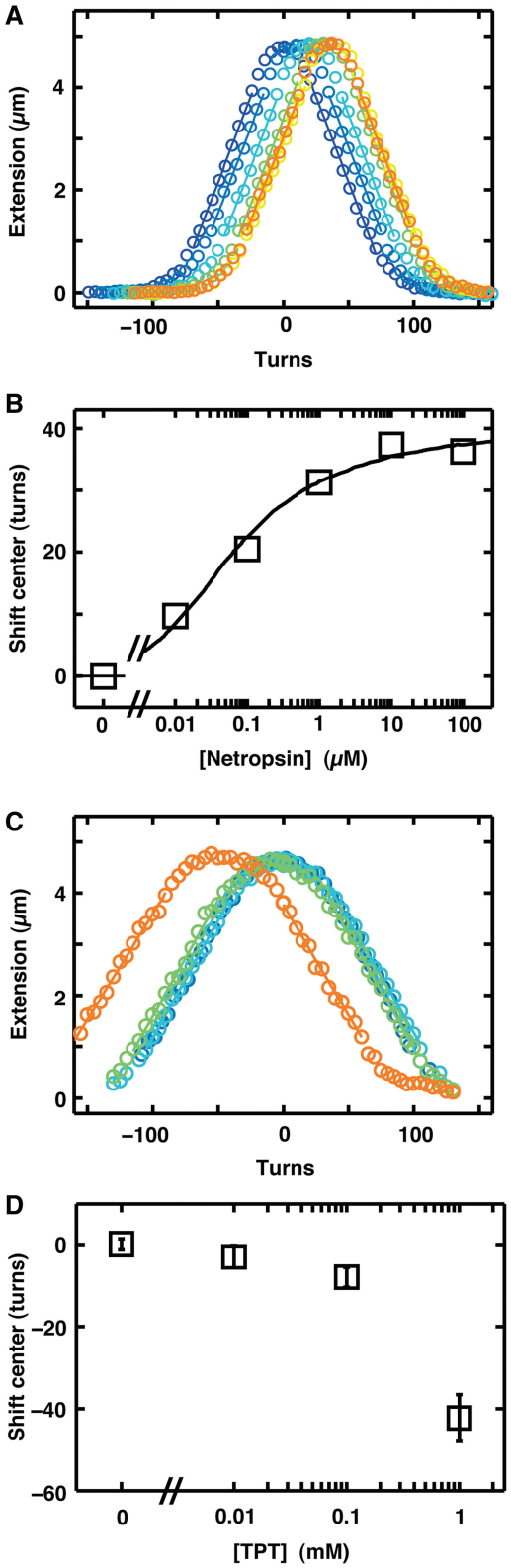

Figure 5. Effect of Netropsin and TPT on DNA rotation–extension behavior at low force. (**A**) Rotation–extension curves for a 20.6-kb DNA in the presence of increasing concentrations of netropsin, taken at $F = 0.25$ pN. Netropsin concentrations employed are (blue to red): 0, 0.01, 0.1, 1, 10 and 100 μM. Upon addition of netropsin, it is observed that rotation of the magnets by positive turns is required to recover the maximum of the rotation–extension curves. (**B**) Quantification of the number of positive turns required to recover the maximum of the rotation–extension curves in the presence of netropsin, as a function of the netropsin concentration (main graph). The black line is a fit to the McGhee–von Hippel model (see main text for details), with binding constant $K = 2.8 \times 10^6\,M^{-1}$ and binding site $n = 11.2$. (**C**) Rotation–extension curves for 20.6-kb DNA in the presence of increasing concentrations of TPT, taken at $F = 0.25$ pN. TPT concentrations employed are (blue to red): 0, 10, 100 and 1000 μM. Upon addition of TPT, it is observed that rotation of the magnets to negative turns is required to recover the maximum of the rotation–extension curves. (**D**) Quantification of the number of negative turns required to recover the maximum of the rotation–extension curves in the presence of TPT, as a function of TPT concentrations. Symbols are the mean and standard deviation from three independent measurements. No binding model was fit to the data since saturation could not be achieved due to the relatively low affinity and limited solubility of TPT.

DNA. This technique can be extended to probe the binding of different types of small molecules. To illustrate the potential for uncovering different binding modes, we have examined the effects of two additional small molecules on the rotational properties of DNA. Addition of the minor groove binder netropsin to rotationally unconstrained dsDNA showed no significant changes in the DNA extension, nor did it significantly influence the value of the bending persistence length (data not shown). However, rotation–extension curves taken on rotationally constrained DNA following the addition of netropsin revealed a shift of the rotation–extension curves (Figure 5A, increasing concentrations of netropsin are shown from blue to red; note that the lack of an effect of netropsin binding on DNA extension can also be observed from this panel). Interestingly, the binding of the minor groove binder netropsin shifts the center of the rotation–extension curves in the opposite direction compared to the shift occasioned by ethidium binding, corresponding to a increase in the twist per base upon netropsin binding. Our observation of an increase in the twist per base upon netropsin binding is in agreement with the findings of bulk solution studies on circular plasmids (31,32,35,66). In contrast, crystal structures of netropsin bound to a short DNA oligomer found no change in DNA twist (34,36). This discrepancy might be due to crystallization artifacts or due to specific effects from the DNA sequence used in the crystallization study. Our single molecule measurements strongly suggest that netropsin does increase the average twist per base when binding to genomic DNA in solution.

Quantification of the number of positive turns required to recover the maximum of the rotation–extension curves in the presence of netropsin, as a function of the netropsin concentration, is shown in Figure 5B. Assuming that binding of one netropsin molecule overwinds the DNA helix by 8°, which is a typical value for the range of values reported from the bulk studies by Snounou and Malcolm (32), this dependence can be fit to the McGhee–von Hippel model in a manner exactly analogous to that employed in the fitting of the EtBr data (Figure 3B), and yields values of $K = 2.8 \times 10^6\,M^{-1}$ for the binding constant and $n = 11.2$ for the binding site. Using the value of 3.5° overwinding per netropsin molecule reported by Triebel *et al.* (35), we obtain a

similar quality fit to the data (not shown) with parameters $K = 6.3 \times 10^6\,M^{-1}$ and $n = 5.1$. A caveat is that netropsin has a known preference for AT-rich sequences (2,32,35). Fitting the simple McGhee–von Hippel binding model, which assumes equivalent binding sites, is therefore a crude approximation to a more complicated binding model that would take into account these preferences. Nonetheless, the data suggest that netropsin has footprint on DNA of at least 5 bp, significantly larger than that of EtBr, in agreement with the crystallographic structure (Figure 1C). In summary, we observe that our technique can also readily inform on the binding of minor-groove binders, despite the fact that they do not have significant effects on DNA extension, in contrast to intercalators such as EtBr.

Effect of the chemotherapeutic topotecan on torsionally constrained DNA

Lastly, we have used our single-molecule rotation techniques to probe the binding of a small molecule for which the binding mode has been disputed, topotecan (TPT). TPT is a topoisomerase IB inhibitor that binds to the topoisomerase IB–DNA complex (67) and can influence the dynamics of supercoil removal (68,69). In previous MT measurement we have detected no effect of TPT on DNA in the absence of topoisomerase in the relatively high ionic strength topoisomerase reaction buffer (50–100 mM monovalent, 1–10 mM divalent ions) for concentrations below 10 μM TPT (68). To test whether TPT binding to bare DNA is detectable by MT, we chose a lower ionic strength buffer (~15 mM monovalent, see Materials and methods section) for this work and tested TPT concentrations up to 1 mM. Measurement at higher TPT concentrations were not possible due to solubility limitations. We observe a clear effect of increasing TPT on rotation–extension curves (Figure 5C). The rotation–extension curves broaden and their centers shift to negative turns (Figure 5B, inset) with increasing TPT concentration, compatible with a reduction in *Tw* as a result of TPT binding. Due to the higher concentrations required to observe an effect on the rotation–extension curves compared to EtBr and netropsin, combined with the solubility limitations that prevent reliable measurements above 1 mM, we were not able to probe TPT binding to DNA up to saturation. Nonetheless, the trends observed upon TPT binding, namely a significant broadening and shift of the rotation–extension curves towards negative turns (Figure 5C), are similar to our observations for ethidium intercalation (Figure 3A). Consequently, our results suggests an intercalative binding mode for TPT.

CONCLUSIONS AND OUTLOOK

In summary, we have employed single-molecule MT that provide rotational control in addition to control of the stretching forces in order to probe the binding modes of small-molecule ligands to DNA. In the case of the intercalator EtBr, studied in greatest detail, these experiments confirm published measurements of the binding constant and binding site size, as well as the reduction of *Tw* occasioned by EtBr binding. They also provide a new means to measure the change in *Tw* caused by the binding of a single ethidium molecule, indicate the possibility of torque-dependent intercalation potentially coupled with a reduction in DNA's torsional stiffness, and demonstrate the stabilization of duplex B-form DNA over single-stranded or P-form DNA by ethidium binding. Our measurements can also readily distinguish between intercalative binding and minor groove binding, allowing one to directly establish the binding mode of a small molecule. As these measurements are performed with magnetic tweezers, which permit multiplexing (70), it is expected that high-throughput versions of these measurements can be implemented in a straightforward manner. Furthermore, the recent augmentation of magnetic tweezers with torque-monitoring capability should in the future complete the analysis of small-molecule binding (71, J. Lipfert *et al.*, submitted for publication).

ACKNOWLEDGEMENTS

The authors thank the members of our laboratory for useful discussions, Jelle van der Does and Dimitri de Roos for machining parts, Jaap Beekman for infrastructural support, and Susanne Hage and Serge Donkers for help with DNA synthesis, Mary-Ann Bjornsti for providing TPT samples, and Francesco Mantegazza for sharing unpublished results from his laboratory.

FUNDING

The Netherlands Organisation for Scientific Research (NWO) via a Veni grant (to JL) and a Vidi grant (to NHD); Delft University of Technology; European Science Foundation via a EURYI award (to NHD). Funding for open access charge: Netherlands Organisation for Scientific Research.

Conflict of interest statement. None declared.

REFERENCES

1. Hendry,L.B., Mahesh,V.B., Bransome,E.D. Jr and Ewing,D.E. (2007) Small molecule intercalation with double stranded DNA: implications for normal gene regulation and for predicting the biological efficacy and genotoxicity of drugs and other chemicals. *Mutat. Res.*, **623**, 53–71.
2. Zimmer,C. and Wahnert,U. (1986) Nonintercalating DNA-binding ligands-specificity of the interaction and their use as tools in biophysical, biochemical and biological investigations of the genetic material. *Prog. Biophys. Mol. Biol.*, **47**, 31–112.
3. Eckel,R., Ros,R., Ros,A., Wilking,S.D., Sewald,N. and Anselmetti,D. (2003) Identification of binding mechanisms in single molecule-DNA complexes. *Biophys. J.*, **85**, 1968–1973.
4. McCauley,M.J. and Williams,M.C. (2009) Optical tweezers experiments resolve distinct modes of DNA-protein binding. *Biopolymers*, **91**, 265–282.
5. Krautbauer,R., Pope,L.H., Schrader,T.E., Allen,S. and Gaub,H.E. (2002) Discriminating small molecule DNA binding modes by single molecule force spectroscopy. *FEBS Lett.*, **510**, 154–158.
6. Cluzel,P., Lebrun,A., Heller,C., Lavery,R., Viovy,J.L., Chatenay,D. and Caron,F. (1996) DNA: an extensible molecule. *Science*, **271**, 792–794.

7. Bennink,M.L., Scharer,O.D., Kanaar,R., Sakata-Sogawa,K., Schins,J.M., Kanger,J.S., de Grooth,B.G. and Greve,J. (1999) Single-molecule manipulation of double-stranded DNA using optical tweezers: interaction studies of DNA with RecA and YOYO-1. *Cytometry*, **36**, 200–208.
8. Sischka,A., Toensing,K., Eckel,R., Wilking,S.D., Sewald,N., Ros,R. and Anselmetti,D. (2005) Molecular mechanisms and kinetics between DNA and DNA binding ligands. *Biophys. J.*, **88**, 404–411.
9. Vladescu,I.D., McCauley,M.J., Rouzina,I. and Williams,M.C. (2005) Mapping the phase diagram of single DNA molecule force-induced melting in the presence of ethidium. *Phys. Rev. Lett.*, **95**, 158102.
10. Vladescu,I.D., McCauley,M.J., Nunez,M.E., Rouzina,I. and Williams,M.C. (2007) Quantifying force-dependent and zero-force DNA intercalation by single-molecule stretching. *Nat. Methods*, **4**, 517–522.
11. McCauley,M.J. and Williams,M.C. (2007) Mechanisms of DNA binding determined in optical tweezers experiments. *Biopolymers*, **85**, 154–168.
12. Mihailovic,A., Vladescu,I., McCauley,M., Ly,E., Williams,M.C., Spain,E.M. and Nu–ez,M.E. (2006) Exploring the interaction of ruthenium(II) polypyridyl complexes with DNA using single-molecule techniques. *Langmuir*, **22**, 4699–4709.
13. Ros,R., Eckel,R., Bartels,F., Sischka,A., Baumgarth,B., Wilking,S.D., Puhler,A., Sewald,N., Becker,A. and Anselmetti,D. (2004) Single molecule force spectroscopy on ligand-DNA complexes: from molecular binding mechanisms to biosensor applications. *J. Biotechnol.*, **112**, 5–12.
14. Tessmer,I., Baumann,C.G., Skinner,G.M., Molloy,J.E., Hoggett,J.G., Tendler,S.J.B. and Allen,S. (2003) Mode of drug binding to DNA determined by optical tweezers force spectroscopy. *J. Mod. Opt.*, **50**, 1627–1636.
15. Paramanathan,T., Westerlund,F., McCauley,M.J., Rouzina,I., Lincoln,P. and Williams,M.C. (2008) Mechanically manipulating the DNA threading intercalation rate. *J. Am. Chem. Soc.*, **130**, 3752–3753.
16. Yang,T.S., Cui,Y., Wu,C.M., Lo,J.M., Chiang,C.S., Shu,W.Y., Chung,W.J., Yu,C.S., Chiang,K.N. and Hsu,I.C. (2009) Determining the zero-force binding energetics of an intercalated DNA complex by a single-molecule approach. *Chemphyschem.*, **10**, 2791–2794.
17. Krautbauer,R., Clausen-Schaumann,H. and Gaub,H.E. (2000) Cisplatin changes the mechanics of single DNA molecules. *Angew. Chemie. Int. Ed.*, **39**, 3912–3915.
18. Wanunu,M., Sutin,J. and Meller,A. (2009) DNA profiling using solid-state nanopores: detection of DNA-binding molecules. *Nano. Lett.*, **9**, 3498–3502.
19. Smith,S.B., Finzi,L. and Bustamante,C. (1992) Direct mechanical measurements of the elasticity of single DNA molecules by using magnetic beads. *Science*, **258**, 1122–1126.
20. Wang,J.C. (1996) DNA topoisomerases. *Annu. Rev. Biochem.*, **65**, 635–692.
21. Champoux,J.J. (2001) DNA topoisomerases: structure, function, and mechanism. *Annu. Rev. Biochem.*, **70**, 369–413.
22. Kouzine,F., Liu,J., Sanford,S., Chung,H.J. and Levens,D. (2004) The dynamic response of upstream DNA to transcription-generated torsional stress. *Nat. Struct. Mol. Biol.*, **11**, 1092–1100.
23. Kouzine,F., Sanford,S., Elisha-Feil,Z. and Levens,D. (2008) The functional response of upstream DNA to dynamic supercoiling in vivo. *Nat. Struct. Mol. Biol.*, **15**, 146–154.
24. Strick,T.R., Croquette,V. and Bensimon,D. (2000) Single-molecule analysis of DNA uncoiling by a type II topoisomerase. *Nature*, **404**, 901–904.
25. Gore,J., Bryant,Z., Nollmann,M., Le,M.U., Cozzarelli,N.R. and Bustamante,C. (2006) DNA overwinds when stretched. *Nature*, **442**, 836–839.
26. Stone,M.D., Bryant,Z., Crisona,N.J., Smith,S.B., Vologodskii,A., Bustamante,C. and Cozzarelli,N.R. (2003) Chirality sensing by Escherichia coli topoisomerase IV and the mechanism of type II topoisomerases. *Proc. Natl Acad. Sci. USA*, **100**, 8654–8659.
27. Allemand,J.F., Bensimon,D., Lavery,R. and Croquette,V. (1998) Stretched and overwound DNA forms a Pauling-like structure with exposed bases. *Proc. Natl Acad. Sci. USA*, **95**, 14152–14157.
28. Strick,T.R., Allemand,J.F., Bensimon,D., Bensimon,A. and Croquette,V. (1996) The elasticity of a single supercoiled DNA molecule. *Science*, **271**, 1835–1837.
29. Lionnet,T., Joubaud,S., Lavery,R., Bensimon,D. and Croquette,V. (2006) Wringing out DNA. *Phys. Rev. Lett.*, **96**, 178102.
30. Langner,K.M., Kedzierski,P., Sokalski,W.A. and Leszczynski,J. (2006) Physical nature of ethidium and proflavine interactions with nucleic acid bases in the intercalation plane. *J. Phys. Chem. B*, **110**, 9720–9727.
31. Malcolm,A.D. and Snounou,G. (1983) Netropsin increases the linking number of DNA. *Cold Spring Harb. Symp. Quant. Biol.*, **47(Pt 1)**, 323–326.
32. Snounou,G. and Malcom,A.D. (1983) Production of positively supercoiled DNA by netropsin. *J. Mol. Biol.*, **167**, 211–216.
33. Finlay,A.C., Hochstein,F.A., Sobin,B.A. and Murphy,F.X. (1951) Netropsin, a new antibiotic produced by a streptomyces. *J. Am. Chem. Soc.*, **73**, 341–343.
34. Kopka,M.L., Yoon,C., Goodsell,D., Pjura,P. and Dickerson,R.E. (1985) The molecular origin of DNA-drug specificity in netropsin and distamycin. *Proc. Natl Acad. Sci. USA*, **82**, 1376–1380.
35. Triebel,H., Bär,H., Geuther,R. and Burckhardt,G. (1995) Netropsin-induced changes of DNA supercoiling; sedimentation studies. *Progr. Colloid. Polym. Sci.*, **99**, 45–54.
36. Kopka,M.L., Yoon,C., Goodsell,D., Pjura,P. and Dickerson,R.E. (1985) Binding of an antitumor drug to DNA, netropsin and C-G-C-G-A-A-T-T-BrC-G-C-G. *J. Mol. Biol.*, **183**, 553–563.
37. Hertzberg,R.P., Caranfa,M.J. and Hecht,S.M. (1989) On the mechanism of topoisomerase I inhibition by camptothecin: evidence for binding to an enzyme-DNA complex. *Biochemistry*, **28**, 4629–4638.
38. Thomas,C.J., Rahier,N.J. and Hecht,S.M. (2004) Camptothecin: current perspectives. *Bioorg. Med. Chem.*, **12**, 1585–1604.
39. Pommier,Y., Pourquier,P., Fan,Y. and Strumberg,D. (1998) Mechanism of action of eukaryotic DNA topoisomerase I and drugs targeted to the enzyme. *Biochim. Biophys. Acta*, **1400**, 83–105.
40. Strel'tsov,S.A., Mikheikin,A.L., Grokhovskii,S.L., Oleinikov,V.A., Kudelina,I.A. and Zhuze,A.L. (2002) [Interaction of topotecan, DNA topoisomerase I inhibitor, with double-stranded polydeoxyribonucleotides. 4. Topotecan binds preferably to the GC base pairs of DNA]. *Mol. Biol. (Mosk)*, **36**, 912–930.
41. Strel'tsov,S.A., Mikheikin,A.L., Grokhovskii,S.L., Oleinikov,V.A. and Zhuze,A.L. (2002) [Interaction of topotecan, DNA topoisomerase I inhibitor, with double-stranded polydeoxyribonucleotides. III. Binding at the minor groove]. *Mol Biol (Mosk)*, **36**, 511–524.
42. Yang,D., Strode,J.T., Spielmann,H.P., Wang,A.H.-J. and Burke,T.G. (1998) DNA interactions of two clinical camptothecin drugs stabilize their active lactone forms. *J. Am. Chem. Soc.*, **120**, 2979–2980.
43. Lipfert,J., Koster,D.A., Vilfan,I.D., Hage,S. and Dekker,N.H. (2009) Single-molecule magnetic tweezers studies of type IB topoisomerases. *Methods Mol. Biol.*, **582**, 71–89.
44. Vilfan,I.D., Lipfert,J., Koster,D.A., Lemay,S.G. and Dekker,N.H. (2009) Magnetic tweezers for single-molecule experiments. In Hinterdorfer,P. and van Oijen,A. (eds), *Handbook of Single-Molecule Biophysics*. Springer, New York, pp. 371–395.
45. Lipfert,J., Hao,X. and Dekker,N.H. (2009) Quantitative modeling and optimization of magnetic tweezers. *Biophys. J.*, **96**, 5040–5049.
46. Bustamante,C., Marko,J.F., Siggia,E.D. and Smith,S. (1994) Entropic elasticity of lambda-phage DNA. *Science*, **265**, 1599–1600.
47. Bouchiat,C., Wang,M.D., Allemand,J., Strick,T., Block,S.M. and Croquette,V. (1999) Estimating the persistence length of a worm-like chain molecule from force-extension measurements. *Biophys. J.*, **76**, 409–413.
48. Forth,S., Deufel,C., Sheinin,M.Y., Daniels,B., Sethna,J.P. and Wang,M.D. (2008) Abrupt buckling transition observed during the plectoneme formation of individual DNA molecules. *Phys. Rev. Lett.*, **100**, 148301.

49. McCauley,M., Hardwidge,P.R., Maher,L.J. 3rd and Williams,M.C. (2005) Dual binding modes for an HMG domain from human HMGB2 on DNA. *Biophys. J.*, **89**, 353–364.
50. Ros,A., Hellmich,W., Duong,T. and Anselmetti,D. (2004) Towards single molecule analysis in PDMS microdevices: from the detection of ultra low dye concentrations to single DNA molecule studies. *J. Biotechnol.*, **112**, 65–72.
51. Coury,J.E., McFail-Isom,L., Williams,L.D. and Bottomley,L.A. (1996) A novel assay for drug-DNA binding mode, affinity, and exclusion number: scanning force microscopy. *Proc. Natl Acad. Sci. USA*, **93**, 12283–12286.
52. McGhee,J.D. and Hippel,P.H.v. (1974) Theoretical aspects of dna-protein interactions: co-operative and non-co-operative binding of large ligands to a one-dimensional homogeneous lattice. *J. Mol. Biol.*, **86**, 469–489.
53. Lerman,L.S. (1961) Structural considerations in the interaction of DNA and acridines. *J. Mol. Biol.*, **3**, 18–30.
54. Hayashi,M. and Harada,Y. (2007) Direct observation of the reversible unwinding of a single DNA molecule caused by the intercalation of ethidium bromide. *Nucleic Acids Res.*, **35**, e125.
55. Berman,H.M. and Young,P.R. (1981) The interaction of intercalating drugs with nucleic acids. *Annu. Rev. Biophys. Bioeng.*, **10**, 87–114.
56. Strick,T., Dessinges,M.-N., Charvin,G., Dekker,N.H., Allemand,J.-F., Bensimon,D. and Croquette,V. (2003) Stretching of macromolecules and proteins. *Rep. Prog. Phys.*, **66**, 1–45.
57. Wang,J.C. (1974) The degree of unwinding of the DNA helix by ethidium. I. Titration of twisted PM2 DNA molecules in alkaline cesium chloride density gradients. *J. Mol. Biol.*, **89**, 783–801.
58. Marko,J.F. (2007) Torque and dynamics of linking number relaxation in stretched supercoiled DNA. *Phys. Rev. E Stat. Nonlin. Soft Matter Phys.*, **76**, 021926.
59. Clauvelin,N., Audoly,B. and Neukirch,S. (2009) Elasticity and electrostatics of plectonemic DNA. *Biophys J*, **96**, 3716–3723.
60. Goyal,S., Perkins,N.C. and Lee,C.L. (2005) Nonlinear dynamics and loop formation in Kirchhoff rods with implications to the mechanics of DNA and cables. *J. Comput. Phys.*, **209**, 371–389.
61. Strick,T.R., Croquette,V. and Bensimon,D. (1998) Homologous pairing in stretched supercoiled DNA. *Proc. Natl Acad. Sci. USA*, **95**, 10579–10583.
62. De Vlaminck,I., Vidic,I., van Loenhout,M.T., Kanaar,R., Lebbink,J.H. and Dekker,C. (2010) Torsional regulation of hRPA-induced unwinding of double-stranded DNA. *Nucleic Acids Res*, Mar 2. [Epub ahead of print]; doi:10.1093/nar/gkq067.
63. Shokri,L., McCauley,M.J., Rouzina,I. and Williams,M.C. (2008) DNA overstretching in the presence of glyoxal: structural evidence of force-induced DNA melting. *Biophys. J.*, **95**, 1248–1255.
64. van Mameren,J., Gross,P., Farge,G., Hooijman,P., Modesti,M., Falkenberg,M., Wuite,G.J. and Peterman,E.J. (2009) Unraveling the structure of DNA during overstretching by using multicolor, single-molecule fluorescence imaging. *Proc. Natl Acad. Sci. USA*, **106**, 18231–18236.
65. Bryant,Z., Stone,M.D., Gore,J., Smith,S.B., Cozzarelli,N.R. and Bustamante,C. (2003) Structural transitions and elasticity from torque measurements on DNA. *Nature*, **424**, 338–341.
66. Triebel,H., Bär,H., Walter,A., Burckhardt,G. and Zimmer,C. (1994) Modulation of DNA supercoiling by interaction with netropsin and other minor groove binders. *J. Biomol. Struct. Dyn.*, **11**, 1085–1105.
67. Staker,B.L., Hjerrild,K., Feese,M.D., Behnke,C.A., Burgin,A.B. Jr and Stewart,L. (2002) The mechanism of topoisomerase I poisoning by a camptothecin analog. *Proc. Natl Acad. Sci. USA*, **99**, 15387–15392.
68. Koster,D.A., Palle,K., Bot,E.S., Bjornsti,M.A. and Dekker,N.H. (2007) Antitumour drugs impede DNA uncoiling by topoisomerase I. *Nature*, **448**, 213–217.
69. Koster,D.A., Czerwinski,F., Halby,L., Crut,A., Vekhoff,P., Palle,K., Arimondo,P.B. and Dekker,N.H. (2008) Single-molecule observations of topotecan-mediated TopIB activity at a unique DNA sequence. *Nucleic Acids Res.*, **36**, 2301–2310.
70. Ribeck,N. and Saleh,O.A. (2008) Multiplexed single-molecule measurements with magnetic tweezers. *Rev. Sci. Instrum.*, **79**, 6.
71. Celedon,A., Nodelman,I.M., Wildt,B., Dewan,R., Searson,P., Wirtz,D., Bowman,G.D. and Sun,S.X. (2009) Magnetic tweezers measurement of single molecule torque. *Nano. Lett.*, **9**, 1720–1725.
72. Humphrey,W., Dalke,A. and Schulten,K. (1996) VMD: Visual molecular dynamics. *J. Mol. Graph.*, **14**, 33–8.